RCF-TESTING OF SELECTIVELY DENSIFIED ROLLERS OF P/M MATERIALS FOR GEAR APPLICATIONS

Pernilla Johansson, Sven Bengtsson and Senad Dizdar

Höganäs AB, Sweden

ABSTRACT

Selective densification can be an appropriate way to fulfill high demands on rolling contact fatigue (RCF) resistance of P/M materials for gear applications. Pre–alloyed P/M materials were tested using the ZF-RCF test. Reference material was low-alloyed case hardened steel DIN 16MnCr5 (AISI 5115) commonly used for gear applications. Test samples, rollers ∅30X30 mm, were pressed from different test materials as cylinders, machined to an oversize compared to the finished roller, selectively densified on a rolling machine and finally heat treated in different ways. The tested rollers were characterized with respect to microstructure, mechanical properties, and surface characteristics. Damage mechanisms were examined and failure analyses were performed on the rollers in order to trace crack initiation and propagation.

INTRODUCTION

Highly loaded sintered components for structural applications are becoming more and more popular in e.g. automobiles. One of the major reasons behind this advance is that in addition to the traditional P/M strong points, cost and dimensional tolerances, the strength and fatigue properties have also been improved. The use of higher densities (>7,2 g/cm^3) through improvements in compaction technology (e.g. Warm compaction) and improvements in powder quality have improved the properties to levels that were previously difficult to reach. One method to reach even higher densities is to densify the P/M body in the areas with the highest load [1-7]. This is particularly efficient for parts subjected to bending loads or high surface pressures, since the stress in the component decreases rapidly from the surface and into the center. One such class of components is gears [1, 4]. The gear root is loaded in bending and failures from fatigue in the tooth root are frequent. Another frequent type of failure is by pitting of the gear flank. By densifying the root and the gear flank to very high or full density the gear life can be improved significantly [1-4, 9].

Failures due to high contact pressures are almost always a fatigue or wear process. A test that simulates the tooth flank wear- and contact fatigue process is the rolling contact fatigue test by Zahnradfabrik Friedrichhafen AG, called ZF-RCF test [10, 11]. In the present work materials aimed for surface densified gear applications are tested in rolling contact fatigue. Since the test method is rather specific to the geometry and running conditions, it is important to compare the test results with data

recorded under similar conditions and with the same equipment [10]. A material frequently used for mass-produced high performance transmission gears is the case hardening steel DIN 16MnCr5 (AISI 5115). This material is used in the present report to benchmark the performance of the surface densified P/M steels.

Rolling contact fatigue tests on PM material have been reported by e.g. [3, 6, 7-9, 11-18]. It can be seen that the improvement in RCF endurable Hertzian pressure with a probability of survival of 50% is strong with increasing density up to a density of about 7,1-7,3 g/cm^3. In some cases [12, 15] it can be seen that the endurable Hertzian pressure drops above this density. At very high densities the endurable Hertzian pressure is higher again [12]. This phenomenon has been reported by [12] and the reason for this behavior is supposed to be the transition from open porosity network to a closed porosity. The open porosity allows the oil to penetrate the porous body without building up a high hydrostatic pressure. In this type of material cracks initiate below the surface and eventually grow towards the surface and cause pitting damage. When the porosity consists of (mainly) closed pores, the hydrostatic pressure can reach very high values just below the surface. In this case the pitting damage starts by cracks initiating at defects at the surface (pores, scratches, etc) followed by oil pressure assisted propagation from the surface towards the interior. Due to the sliding action (friction) the cracks propagate at an angle (approximately 30^o) from the radial direction. The cracks eventually link up to form a pitting damage.

The present work aims at investigating the rolling contact fatigue behavior of some selectively densified materials and compare with a wrought reference material.

EXPERIMENTAL

Four fully pre-alloyed base powders were used in this study, Astaloy Mo, Astaloy A, Astaloy 85Mo and Astaloy CrL as shown in Table I. The first material has been used in a previous study [18] and is included as a reference. The requirements on materials for surface densification have been discussed in e.g. [4, 6, 19].

Table I. Composition of the investigated materials (weight %).

Code	Material	Standard designation	%Gr	%Cr	%Ni	%Mo	%Mn	%Si
A	Astaloy Mo	-	0.60	-	-	1.50	0.10	-
B	Astaloy A	4600	0.30	-	1.9	0.55	0.20	-
C	Astaloy 85 Mo	4400	0.20	-	-	0.85	0.10	-
D	Astaloy CrL	-	0.25	1.50		0.50		
R	DIN 16MnCr5 / AISI 5115		0.16	0.80	-	-	0.8	0.25

Test samples were prepared as ZF-RCF rollers ∅30X30 mm from test materials as above. The rollers were first pressed as ∅31mm cylinders to a density between 7.0 and 7.2 g/cm³ as shown in Table III. The sintering was performed in a mesh belt furnace at 1120 ^{o}C (2050 ^{o}F) in a mixture of 90% N_2 and 10% H_2 for 30 minutes. The specimens were then turned into a shape slightly larger than the desired specimen geometry. The sintered rollers were machined to a slight oversize compared to the finished roller as shown in Table III.

The rollers were then densified in a rolling machine and finally heat treated in different ways. All the materials except D were case hardened using standard equipment and endo-gas type atmosphere. Material D requires the use of low-pressure carbonization due to its sensitivity to oxidation. Material B was divided into two groups: the first, B1, was case hardened in a standard way using a solution temperature of 920 °C (1688 °F) and an appropriate soaking time to produce the case depth of 0.5 mm. After the solution treatment the rollers were quenched in oil bath at 80 °C (172 °F). A temper-

ing at 160 °C (320 °F) for 60 min followed the treatment. The B2 material was first heat treated in the same way as B1 and then case hardened again using the same parameters except for the solution treatment time that was adjusted so that the total time (including treatment 1) should give a case depth between 1,5 and 2 times that of the first treatment. (B1).

The rolling contact fatigue test used here is an accelerated type test described by e.g. [10-12]. The test bench is schematically shown in Figure 1. A test roller specimen comes into contact by three counter load rollers, shifted by 120°, so that the loading frequency is three times the rotational velocity. A hydraulic loading system presses the counter rollers onto the specimen and in this way provide the normal contact loading. A gear drive adjusts the relative sliding between the specimen and counter rollers. An accelerometer is fitted to the machine structure. When a piece of material falls off from the specimen it causes a vibration that the accelerometer records. When the vibration level exceeds a preset value the machine is stopped.

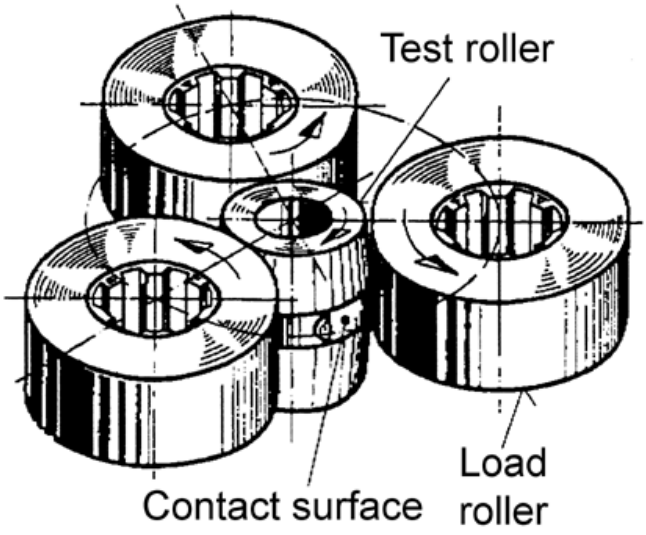


Figure 1. A schematic view of the test and load roller in the contact [12].

Table II. RCF-test particulars.

Specimen roller diameter	d= 30 mm $R_a \leq 0.2$ µm,
Load roller	D = 70 mm $R_a \leq 0.50$ µm, $R_q \leq 0.65$ µm, $R_{max} \leq 2.0$ µm (ground surface)
Line contact width	5±0.1 mm
Hertzian pressure	1400-2500 MPa (calculated for E = 206 000 MPa) (203-362 ksi)
Load frequency	$72s^{-1}$ (1440 RPM)
Relative sliding	- 24% (0.535 m/s)
Lubricated oil	Gearbox oil SAE 80W EP API GL-4, MIL-L-2105, FZG A/8.3/90: >12
Oil temperature	80°C

A test run is terminated when run-out or one of RCF-failure criteria i.e. pitting, excessive wear rate or excessive crack propagation has occurred. A run-out is defined as a specimen running more than 20 million cycles without causing a pitting damage that is large enough to stop the machine. Normally a few tests are performed at two levels where failure is ensured and one level close to the 50% endurable Hertzian pressure. Once the finite life curve is established it is possible to either run a few

at a safe level or to start a staircase evaluation (in case of failure decrease the load of the next specimen; in case of a run-out increase it). In order to find an approximate level of the performance of a material, approximately 15 points are needed. Some further details of the RCF testing are found in Table II.

The tested samples were examined with respect to surface roughness and wear mechanisms. The appearance of the pitting damage was visually investigated. By using metallography, the microstructure of the tested rollers was assessed. Hardness tests were used to characterize the case hardening.

RESULTS

The densification of the rollers was examined using metallography. Figure 2 shows the density distribution in the axial plane. The densified layer extends outside the loaded surface. The densification in the radial direction can be seen as dotted lines in Figure 3. Material C has the deepest densification of all the materials. It is followed by materials D, A and B in that order. Selected densification parameters and densification depth are shown in Table III. The densification depth is defined as the distance from the surface to where the density drops below 98% of full theoretical density.

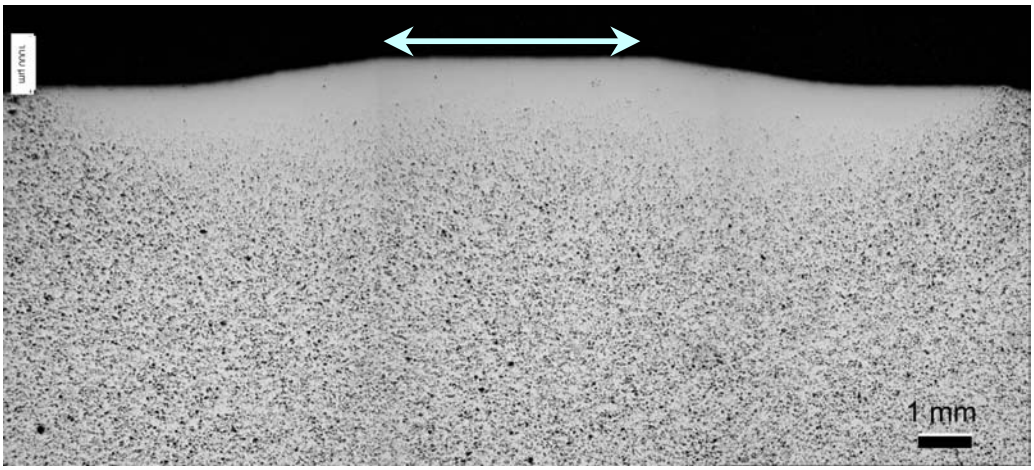


Figure 2. Metallography of an axial section of material C, Astaloy 85Mo + 0.2%C, in the as-polished condition. The contact track is the 5 mm wide flat (cylindrical) section seen at the top center.

It should be recognized that if the pitting damage initiates at a pore near the surface, a very low number of pores are sufficient to lower the endurable Hertzian pressure significantly. The number of such pores is very difficult to measure reliably using automatic image analysis methods. Instead, the amount and character of these pores were compared and ranked as shown in Table IV. In this table, observations on the changes in microstructure that occur during the testing are described.

Table III. Selected properties of the investigated materials.

Code	Material	Standard designation	SD (g/cm³)	Over measure (mm) (inch)	Densification depth (mm) (inch)	Case depth (mm) (inch)	Surface hardness HV0.1
A	Astaloy Mo	-	7.2	0.3 (0.013)	0.9 (0.35)	-*	940
B1	Astaloy A	4600	7.2	0.3 (0.013)	0.8 (0.032)	0.50 (0.020)	880
B2					0.8 (0.032)	0.75 (0.029)	830
C	Astaloy 85 Mo	4400	7,0	0.5 (0.020)	1.2 (0.047)	0.75 (0.029)	949
D	Astaloy CrL	-	7,0	0.5 (0.020)	1.1 (0.043)	0.70 (0.028)	900
R	DIN 16MnCr5 / AISI 5115		7.9	-	-		

* Core hardness > 600 HV0.1.

As seen in Table III and Figure 3 a-d the case depth is around 0.70-0.75 mm for all the specimens except A and B1. This case depth correlates to the "rule of thumb" that says that the case depth should be approximately 0.15 – 0.20 times the normal module. The present roller test corresponds to a module of 4, thus requiring a case depth of 0.6 – 0.8 mm. The case depth of the B1 material is on the low side, but actually still within the normal tolerances of ±0.2 mm. The material A with its higher carbon content in the core is always above 550 HV0.1 so a case depth cannot be defined. The surface hardness varies between 930 HV0.1 for the materials A and C to 810 HV0.1 for the B2 material. This material has been subjected to a double heat treatment and it is evident that although carbonization was achieved, the surface and core hardness dropped compared to B1. The scatter in the micro hardness is associated with the homogeneity of the microstructure. Material A has a very uniform martensitic microstructure at the surface and consequently a low scatter. The scatter increases as bainite starts to form deeper into the material. The scatter in hardness is high at the surface and in the core for the B1 and B2 materials. At the surface this is believed to be caused by the presence of retained austenite, while the scatter deeper into the material again is associated with the formation of bainite.

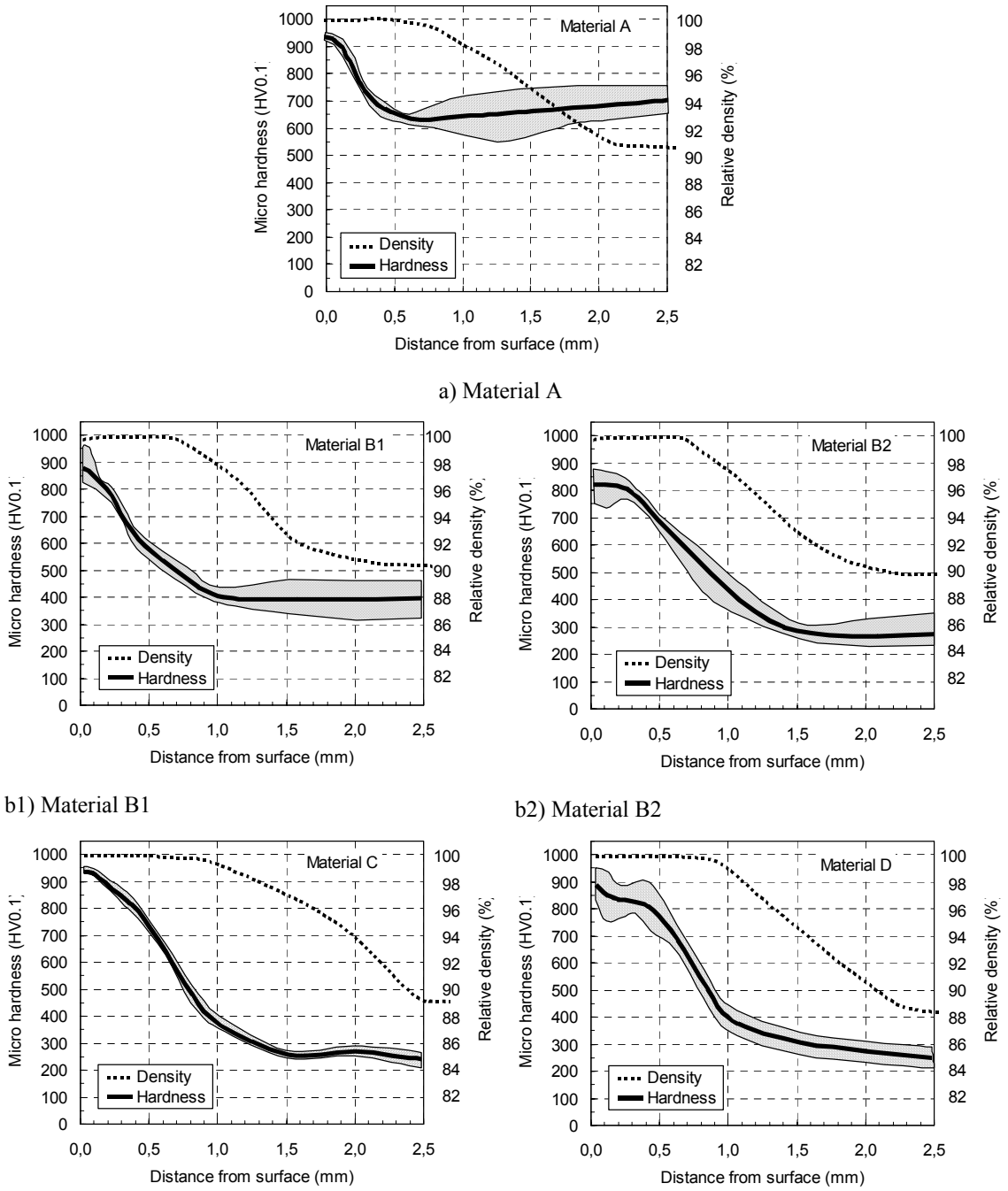


Figure 3. Combined micro hardness profile and density distribution diagram for material D. The solid line indicates the micro hardness (HV0.1). The shaded area is the ±1σ scatter band. The broken line shows the local relative density measured by image analysis.

Material C has a low scatter at all depths from the surface. The reason for this low scatter is not clear. However, the microstructure at the surface is martensitic with some retained austenite. At some distance from the surface bainite starts to form. Material D is different from the others in that it was case hardened using a low-pressure carbonization method followed by gas quenching. However, the microstructure follows the same pattern as the others with the exception that a few carbides are

found in the region near the surface. At the surface the scatter in hardness is relatively high, a fact that is attributed to the presence of retained austenite, and carbides in the martensite. Further into the material the scatter decreases and remains at a relatively low level.

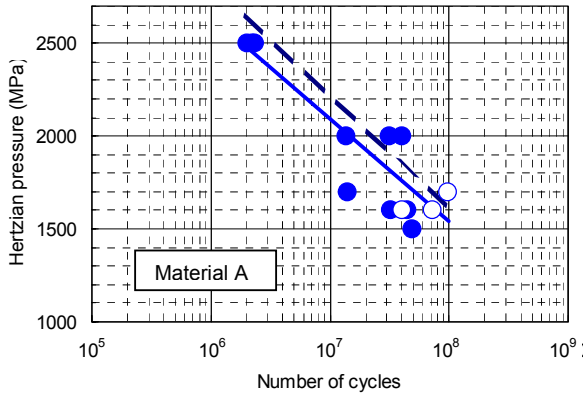
Figure 4 shows the S/N diagram of material A-D. In diagram 4a it can be seen that the regression line for the material A is quite close to the reference material. The endurable Hertzian pressure at 100 10^6 cycles reaches 1550 MPa compared to the 1600 MPa for the reference. The performance of the two materials B1 and B2 is remarkably similar taking into account the difference in case depth, as can be seen in Figures 4b1 and 4b2. It appears that the B2 material is better but considering the low number of tests this is not an undisputable fact. Furthermore, the B2 material exhibits a different failure mechanism for some of the rollers. Large breakouts are formed instead of the ordinary pitting damage. Material C exhibits a lower endurable Hertzian pressure compared to the other materials. The number of tests is not sufficient to establish an endurable Hertzian pressure with an acceptable degree of confidence but around 1200-1400 MPa is a likely level. The number of tests for the material D is even smaller, making any definite statements on the endurable Hertzian pressure difficult, but this material should be somewhat higher compared to material C.

The failure criterion used when running the tests is that a surface pit is formed that is large enough to cause vibrations that exceed a pre-set level. Figure 5 shows typical pitting damage for the tested materials. All specimens failed through pitting damage. The typical pitting damage is almost as wide as the contact surface and usually extends a small distance outside the contact surface (Figure 5 a-f). However, the material B2 shows two types of pitting as shown in Figure 5c. Damage that is of the same size as the other materials and in a few cases a breakout of material that is very much larger than the normal pitting. This damage is approximately twice as deep as the normal damage and runs below the densified zone and extends outside the densified region.

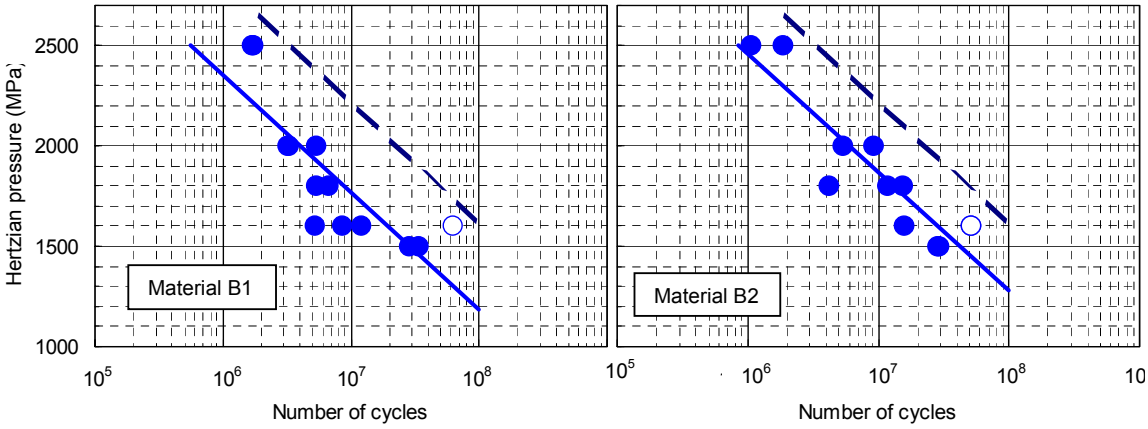
The observations of porosity near the surface and of microstructural changes during testing are summarized in Table IV. From the metallographic investigation stresses and temperature induced phase transformations, so-called butterflies were found in all materials except in material A. It is generally observed that there are a higher number of butterflies and especially a higher number of large butterflies for a higher load compared to a lower load. The butterflies can be divided into three different groups where the two first ones appear in all materials and the third one only appears in material D. The first group consists of very small butterflies of a size of ~5 μm and they appears at a depth at 0.05-0.25 mm from the surface as shown in Figure 6a. They mainly appear in connection with a pore. The second group of butterflies is somewhat larger, around 15-35 μm in size, and is usually found deeper into the roller at a depth of 0.25-0.8 mm from the surface. They also appear in connection with pores or cracks as shown in Figure 6b. In materials B2 and C pore clusters were found in the densified zone and it was at these pores the butterflies were found. Figure 6c shows both small and large butterflies in a cluster zone of material C. The third group of butterflies appears in connection with dark areas in the martensite. These areas have the appearance (and hardness) of lower bainite, but have been formed during the testing. Figure 6d shows the transformed material in the vicinity of a butterfly.

Table IV. Microstructural observations on the tested materials.

Material Load, no. of cycles	**Surface porosity**	**Micro structural features**
A 1600 MPa, 43,8 10^6 cycles	Intermediate number of near surface pores. Ranked as no 3.	A few carbides are found in the near surface region. The shape is relatively round and they are usually isolated, but located in the grain boundaries. No butterflies or other microstructural changes due to the testing are found in these specimens.
B1 2500 MPa, 1.7 10^6 cycles	Intermediate number of near surface pores. Ranked as no 2. The pores appear in clusters. The effect is not as strong as in B2 and C.	Butterflies are found 0.05 to 0.5 mm below the surface. They are found both at pores and at cracks. The butterflies found at the surface are small (≈5 μm) while they are larger further into the roller. A few long and very long butterflies are found near cracks.
B1 1600 MPa, 12 10^6 cycles		Butterflies are found 0.05 to 0.5 mm below the surface. They are found both at pores and at cracks. The butterflies found at the surface are very small (≈5 μm) while they are larger (15-35 μm) further into the roller.
B2 2500 MPa, 1.9 10^6 cycles	Intermediate number of near surface pores. Ranked as no 4. The pores appear in clusters.	Butterflies are found 0.1 to 0.8 mm below the surface. They are found both at pores and at cracks. The butterflies are relatively small (≈5 μm). Large butterflies are found near cracks (50 μm or larger).
B2 1600 MPa, 51 10^6 cycles		Butterflies are found 0.05 to 0.25 mm below the surface. They are found both at pores and at cracks. The butterflies found at the surface are very small (≈5 μm) while they are larger (15-30 μm) further into the roller.
C 2000 MPa, 1.7 10^6 cycles	Highest number of near surface pores. Ranked as no 5. The pores appear in clusters. The clustering effect is strong.	Butterflies are found 0.1 to 0.5 mm below the surface. They are found both at pores and at small cracks. They are associated with the pore clusters. The size varies from small to large.
C 1600 MPa, 19 10^6 cycles		Butterflies are found 0.03 to 0.35 mm below the surface. They are found both at pores and at small cracks. The butterflies found at the surface are extremely small (<5 μm) while they are larger (15-35 μm) further into the roller.
D 2000 MPa, 1.7 10^6 cycles	Lowest number of near surface pores. Ranked as no 1.	In this material the butterflies are associated with another microstructural change. It appears as if the martensite breaks down into a structure with the appearance of lower bainite. At these sites butterflies can be found. It is possible that small cracks exist at these positions. A few carbides were found near the surface.

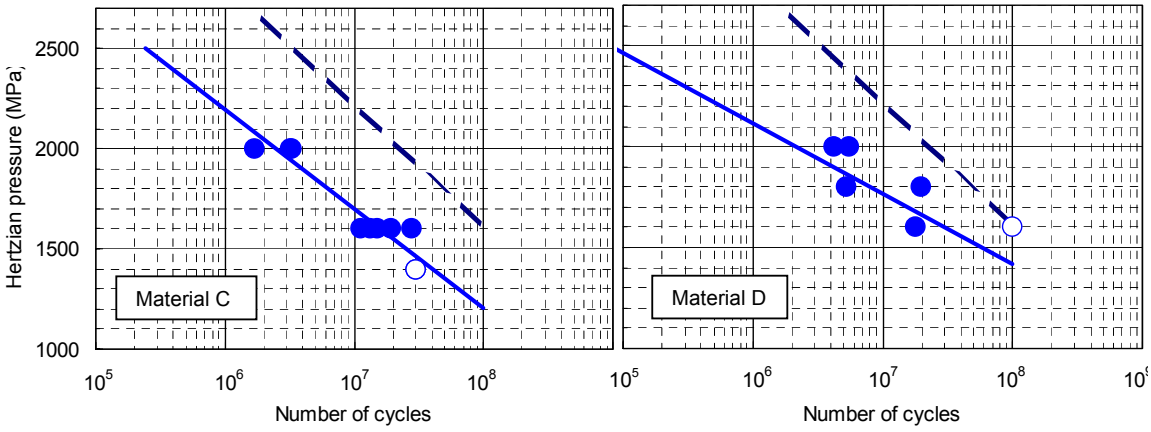


a) Material A.



b1) Material B1.

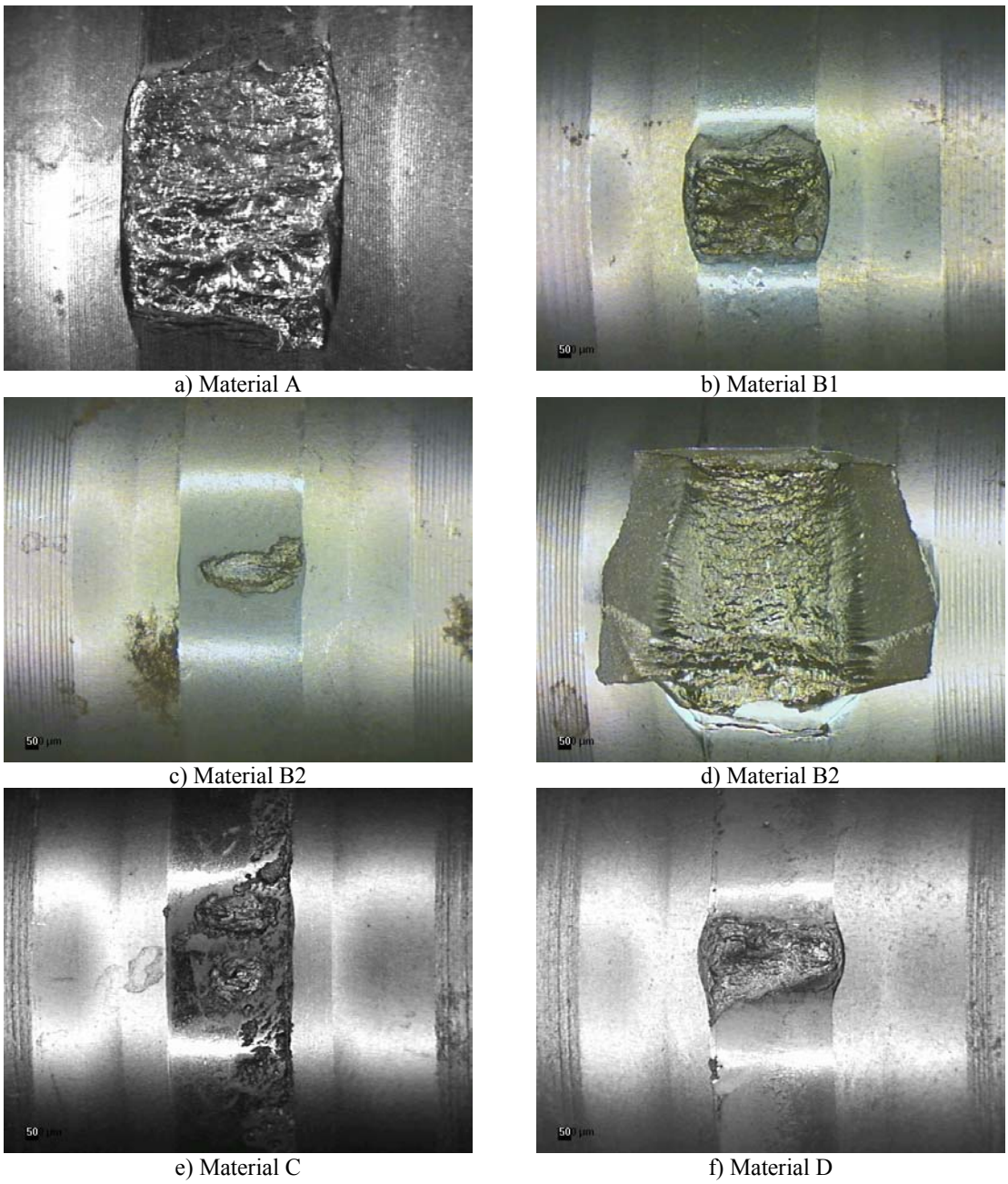
b2) Material B2.



c) Material C.

d) Material D.

Figure 4. S/N curve of the tested materials. The filled circles indicate failures while the open circles show run-outs. The solid line is a regression line through all the points. The performance of the reference material DIN 16MnCr5 (AISI 5115) is indicated by the broken line.



a) Material A b) Material B1

c) Material B2 d) Material B2

e) Material C f) Material D

Figure 5. Macro photograph of typical pitting damage on the tested materials. The tested contact surface is seen as a vertical band. This band is approximately 5 mm wide. Notice that a) is at a higher magnification

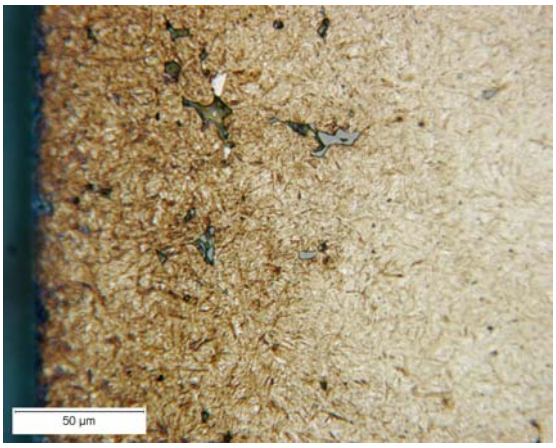
DISCUSSION

Material A exhibits the best RCF performance of the tested materials. There are two factors that are unique for this material. The core hardness is much higher (400 HV0.1) compared to the other materials (~270 HV0.1). This material does not exhibit any stress and temperature induced phase transformation. It is not possible, with the available material, to unambiguously identify the reasons or mechanism responsible for the good performance.

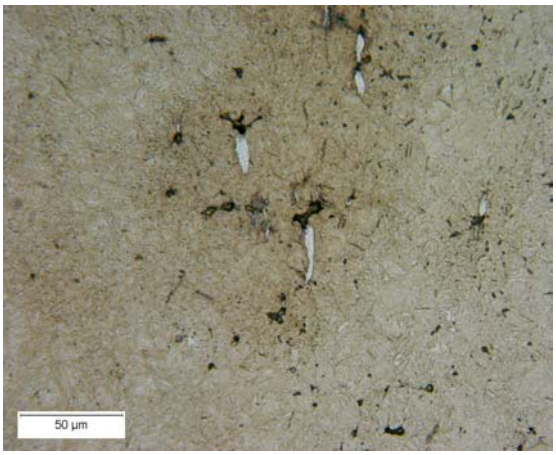
It was anticipated that the deeper case depth of B2 compared to B1 would give a better endurable Hertzian pressure. However, it appears that this is not the case. Several factors may have a significant influence on this behavior. If both the heat treatments are considered the carbonization of B2

was performed totally four times as long as B1 in total. In theory, this should result in a case depth twice as deep as B1. In reality only a 50% increase was achieved. The reasons behind this apparent lack of carbonization could be a factual lower carbonization rate in the second heat treatment. The microstructure is very similar in the two cases considering the deeper carbonization of B2, it appears reasonable to attribute the lower hardness to a higher degree of tempering. It can be speculated that the large breakouts found in the B2 material could be attributed to the soft-core material, since the crack path was just inside the densified layer.

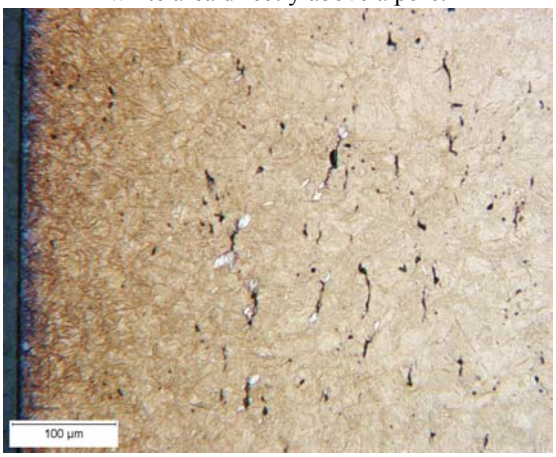
Another factor that reinforces the danger with a low ratio between densification depth and case depth is the residual stresses formed during the heat treatment. If the densification depth is much larger than the case depth the compressive stresses generated by the case hardening in the near surface zone can be balanced by tensile stresses inside this zone. However, if the densification is to shallow, the compressive stresses will form in the densified layer, leaving the un-densified material inside this layer to cope with the tensile stresses. These stresses are lower in magnitude compared to the compressive stresses closer to the surface, but spread over a larger volume. During testing this area will undergo a stress cycle that shifts from positive to negative stresses, albeit at a lower absolute level compared to the near surface region.



a) Material B1, small butterfly. The butterfly is the white area directly above a pore.



b) Material B1, “Large” butterflies located at pores.



c) Material C, the butterflies are white spots directly associated with the pores and cracks



d). Material D, the butterfly is the white area in the center of the micrograph. Typical dark areas are found near the butterflies

Figure 6. Metallographical views on butterflies near the surface of rollers. The butterflies are the white spots/areas. Etched in nital/picral.

The performance of material C is somewhat of a disappointment. It has the deepest densification of all the tested materials. The desired carbonization profile was accomplished and the surface hardness is among the highest. All these factors should contribute to a good rolling contact performance. However, although the total amount of residual porosity near the surface is very low, it tends to form clusters. It has been observed that butterflies tend to form in these clusters, possibly acting as an initiation site for cracks. By comparing with material A it can be noted that material C is harder from the surface and approximately 0.6 mm into the roller. In other words material C is harder in the region where crack initiation and propagation takes place. The depth of densification is in both cases sufficient to support the outer carbonized layer. However, in the case of material A the residual porosity is relatively uniformly distributed in contrast to the clustering of material C. The reasons for the clustering are at this point not clear.

Although Material D exhibits a moderate endurable Hertzian pressure of 1400 MPa it is believed that this figure could be improved by performing a better case hardening cycle. Carbides where found near the surface of the rollers. By a better control over the carbonization cycle these carbides can be avoided without loosing surface hardness. Adding more graphite into the powder mix could also raise the core hardness. In this material dark areas are found at the butterflies. The appearance of these areas looks like lower bainite in the optical microscope. However, it has not been possible to identify the phases present in the dark areas.

CONCLUSIONS

An optimized case hardening process is very important for the endurable Hertzian pressure. A high surface hardness, optimum carbon profile and relatively high core hardness are important parameters. The near surface region must be free from carbides, oxides, slag and pore clusters.

- Material A, Astaloy Mo, exhibits the highest endurable Hertzian pressure among the tested materials. It reaches 1550 MPa.
- Material D, Astaloy CrL, reaches the second highest endurable Hertzian pressure reaching a value of approximately 1500 MPa.
- The presence of pores or pore clusters near the surface is very detrimental for the endurable Hertzian pressure.
- Astaloy Mo does not exhibit a phase transformation that can be associated with the initiation of cracks that eventually form pitting damage.
- For material B, Astaloy A, and material C, Astaloy 85Mo, the formation of butterflies is associated with the breakdown of the martensitic microstructure and eventually with crack initiation. Most of these butterflies nucleate at pores or small cracks.
- In addition to the normal appearance of the butterflies found in Material D, Astaloy CrL, a dark region with the appearance of lower bainite can be found.

ACKNOWLEDGEMENTS

The authors are very grateful to Dr Lipp at the Fraunhofer Institute in Darmstadt. His skill and helpfulness are deeply appreciated..

REFERENCES

1. Y. Takeya, T. Hayasaka, M. Suzuki, ”Surface Rolling of Sintered Gears”, SAE International Congress and Exposition, Detroit, Michigan, February 22-26, 1982, Paper No 820234.
2. C.M. Sonsino, G. Schlieper, J. Tengzelius, “Influence of as-sintered material strength on the improvement of fatigue behaviour by surface rolling”, In: Powder Metallurgy 90, July 2-6, (1990)

3. T.M. Cadle, C.J. Landgraf, P. Brewin, P. Nurthen, "Rolling Contact Fatigue Resistance of P/M Steel--Effects of Sintering Temperature and Material Density", *Advances in Powder Metallurgy--1991*. Vol. 1, Chicago, Illinois, USA, 9-12 June 1991, pp175-182

4. P.K. Jones, K. Buckley-Golder, R. Lawcock, R. Shivanath, "Densification strategies for high endurance P/M components", International Journal of Powder Metallurgy, vol 33, no 3, (1997), pp 37-44.

5. E. Broszeit, H. Steindorf, G. Schlieper, "Surface rolling of sintered materials", Int. Powder Metallurgy Conference, 1986, Düsseldorf, pp403-406.

6. S. Nigarura, P. Blanchard and J. Trasorras, "Processing Effects on rolling contact fatigue properties of sintered and Densiformed ferrous alloys", 2001 International Conference on Powder Metallurgy & Particulate Materials", New Orleans, May 13-17, 2001, pp10.16-10.35.

7. S. Bengtsson and L. Fordén, "Rolling contact fatigue tests of selectively densified materials", 2001 International Conference on Powder Metallurgy & Particulate Materials", New Orleans, May 13-17, 2001, pp10.71-10.86.

8. C.M. Sonsino, G. Schlieper, W.J. Huppmann, "How to improve the fatigue properties of sintered steels by combined mechanical and thermal surface treatments", Int. Powder Metallurgy Conference, June 17-22 (1984), Toronto, Canada

9. P.K. Jones, K. Buckley-Golder, H. David, R. Lawcock, D. Sarafinchan, R. Shivanath, L. Yao, "Fatigue Properties of Advanced High Density Powder Metal Alloy Steels for High Performance Powertrain Applications", *Powder Metallurgy World Congress and Exhibition*, Vol 3., October 18-22, 1998, Grenada, Spain, pp155-166.

10. Beschreibung des Rollenprüfstandes VA 2709, ZF Friedrichschafen AG, Friedrichschafen, Germany, 1967.

11. G. Hoffmann, K. Lipp, K. Michaelis, C.M. Sonsino J.A. Rice, "Testing P/M materials for high loading gear applications", Int. J. Powder Met., 35/6, (1999), pp. 35-44.

12. K. Lipp, "Oberfläschenzerrüttung von Sinterstählen unter Konstanter und veränderlicher Herzscher Pressung mit überlagerter Reibung (Schlupf)", 1997, Ph.D. Thesis, Fraunhofer Institut für Betriebsfestigkeit, Darmstadt, Germany.

13. H. Hirata, S. Kigushi, M. Wada, S. Oda, T. Koide, T, "Load bearing capacity of ferrous sintered gears", Japan Society of Powder and Powder Metallurgy; 1993; pp1051-1054

14. R. Strehl, "Tragfähighkeit von Zahnrädern aus Hochfesten Sinterstählen", 1997, Ph.D. Thesis, Reinisch-Westfälischen Technischen Hochschule Aachen, Aachen, Germany

15. K. Lipp, C.M. Sonsino, D. Pohl, S. Hock, "Rolling Contact Fatigue Behaviour of Sintered Steels – Endurable Hertzian Pressures and Damage Mechanisms", ", Powder Metallurgy World Congress and Exhibition, Vol 3., October 18-22, 1998, Grenada, Spain, p143-148.

16. J. Petersen and P. Beiss, "The influence of the core carbon content on the rolling contact fatigue of Distaloy HP-1", 2001 International Conference on Powder Metallurgy & Particulate Materials", New Orleans, May 13-17, 2001, pp10.36-10.50.

17. G. Straffelini, A. Molinari, Effects of hardness on rolling-sliding damage mechanisms in PM alloys, Powder Metallurgy, 44 (2001) 344-350

18. G. Straffelini, T. Marcu Puskas, A. Molinari, Identification of rolling sliding damage mechanisms in porous alloys, Metallurgical and materials transactions A, 31A (2000) 3091-3099.

19. S. Bengtsson, S. Dizdar and M. Svensson, "Material aspects of selectively densified transmission gears", 2000 Powder Metallurgy World Congress, Eds K. Kosuge, H Nagai, Nov 12-16, 2000, pp967-970.